Root-Type-Specific Water Uptake in Maize across Soil Texture and Moisture Gradients

Ruth Adamczewski[1], Anders Kaestner[2], Johanna Pausch[3], Maire Holz[4], Mohsen Zarebanadkouki[1]

[1] Soil Biophysics and Environmental Systems, School of Life Science, Technical University of Munich, Freising, Germany

[2] PSI Center for Neutron and Muon Sciences, Paul Scherrer Institute, Villigen, Switzerland

[3] Agroecology, Bayreuth Center of Ecology and Environmental Research (BayCEER), University of Bayreuth, Bayreuth, Germany

[4] Leibniz Centre for Agricultural Landscape Research (ZALF), Müncheberg, Germany

Correspondence to: ruth.adamczewski@tum.de, Mohsen.zare@tum.de

Abstract

Understanding how distinct root types contribute to water uptake under variable soil conditions is crucial for improving crop water use efficiency. We quantified root water uptake in six-week-old maize grown in sandy or loamy soil under well-watered and water-limited conditions. Time-series neutron radiography combined with deuterated water labelling enabled estimation of effective radial water uptake of crown and seminal roots using a diffusion–convection model.

Plant development responded strongly to the soil environment, with the greatest reductions in transpiration, shoot height, and root length occurring under sandy-dry conditions. Root water uptake patterns varied with soil texture and water availability. Crown roots exhibited pronounced hydraulic plasticity, with radial fluxes approximately threefold higher in sandy than in loamy soil. In contrast, seminal roots showed no impact of soil conditions on root water uptake. Overall, crown roots showed two times higher radial fluxes than seminal roots.

These findings demonstrate how soil texture and moisture interact with root-type-specific hydraulic function, providing insights for breeding and modelling drought-resilient maize.

https://doi.org/10.5194/egusphere-2026-1740
Preprint. Discussion started: 29 April 2026

1 Introduction

Understanding how plants acquire water from soil is fundamental to predicting their responses to environmental stress, particularly under water-limited conditions. Root water uptake (RWU) is governed by complex interactions between root traits and soil hydraulic properties, which together determine the spatiotemporal dynamics of water flow to roots. In moist soils, water flow is mainly limited by root hydraulic resistance, whereas in drying soils, soil hydraulic resistance becomes increasingly dominant, constraining RWU (Carminati and Javaux, 2020; Draye et al., 2010; Steudle, 2000). The decline in soil hydraulic conductivity with decreasing matric potential is strongly texture-dependent. Coarse-textured sandy soils exhibit a sharp drop in conductivity over a narrow range of matric potentials, while fine-textured soils show a more gradual reduction, with profound implications for water availability and plant function (Draye et al., 2010; Hohenbrink et al., 2023; Wankmüller et al., 2024). These contrasting soil hydraulic properties shape plant root strategies. Plants balance the carbon costs of root development and maintenance against the efficiency of water and nutrient uptake (Bassiouni et al., 2023; Guswa, 2008). For instance, maize (*Zea mays*) typically produces longer, finer roots with greater active length in loamy soils, while in sandy soils, roots tend to be shorter and thicker, which is most likely a cost-benefit adjustment but not yet proven (Cai et al., 2021; Lippold et al., 2021).

Cereals have two main types of fibrous roots: (i) seminal axial roots (primary and seminal), which are of embryonic origin, and (ii) nodal axial roots (crown and brace), which form post-embryonically from stem nodes. Both types produce lateral roots that branch perpendicularly and may develop root hairs to increase surface area (Hochholdinger et al., 2004). In maize, architectural adaptations such as fewer but longer lateral roots and fewer crown roots have been shown to increase rooting depth, reduce metabolic costs, and enhance drought tolerance and nutrient acquisition (Lynch et al., 2024; Zhan et al., 2015). These traits facilitate C reallocation to deeper rooting zones, supporting water uptake under limiting conditions (Lynch, 2013; Zhan et al., 2015). Under controlled conditions, experimental studies have shown that during early developmental stages and in sandy, well-watered soils, water uptake is predominantly driven by the primary and lateral roots, whereas in older plants (five weeks), crown roots play a more prominent role in water acquisition (Ahmed et al. 2016, 2018; Tötzke et al. 2021). Given the structural and functional complexity of root systems, it is critical to understand their adaptive significance and the relative contribution of individual root types and segments to water and nutrient uptake, especially under water deficit conditions. Since distinct root classes exhibit differential access to water resources (Klein et al. 2020; Ahmed et al. 2018), a key question remains whether plants selectively promote elongation or development of specific root types to enhance water acquisition in heterogeneous soil environments.

Despite significant advances in modeling and imaging technologies, the in-situ quantification of RWU remains a major challenge due to the opaque and heterogeneous nature of soil. Early studies primarily investigated RWU in hydroponic systems, simplifying the system by the influence of soil on water uptake dynamics (Frensch et al., 1996; Steudle, 2000). More recent research has increasingly recognized RWU as a dynamic, interactive process between roots and their surrounding soil environment (Moradi et al. 2011; Carminati et al. 2016). The development of non-invasive imaging techniques, such as fast neutron tomography and radiography using deuterated water (D_2O) tracers, now enables high-resolution, time-resolved visualization of water fluxes within root systems under realistic soil conditions (Tötzke et al. 2021; Zarebanadkouki et al. 2012; Hayat et al. 2020; Warren et al. 2013). When combined with inverse modeling, these approaches allow for the spatially resolved quantification of local RWU across root types and developmental stages (Zarebanadkouki et al., 2012, 2013; Ahmed et al., 2016, 2018). This has provided novel insights into key processes, including hydraulic redistribution (Hayat et al., 2020), hydraulic conductivities of the root-soil interface (Zarebanadkouki, et al. 2016a), root hydraulic conductivity (Zarebanadkouki, et al. 2016b), as well as capturing 3D water flow in rooted soil by ultra-fast neutron tomography and water transport through the root at the cellular scale (Zarebanadkouki et al. 2019).

However, despite these methodological advances, the influence of contrasting soil textures on the spatial distribution and dynamics of RWU in maize remains insufficiently understood. Specifically, it is unclear how soil texture interacts with water availability to shape root functional responses and water acquisition patterns. The objective of this study was to investigate RWU in maize grown in two contrasting soil textures - sandy (S) and loamy (L) - under both well-watered (W) and water-deficit (D) conditions. Specifically, we aimed to: (i) characterize the number, length, and radius of distinct root types under varying soil and moisture conditions; (ii) quantify differences in RWU patterns between soil types and assess the influence of water availability on uptake dynamics, through the integration of high-resolution imaging, isotopic tracing, and inverse modeling; and (iii) quantify how RWU varies along the root axis as a function of distance from the tip under contrasting soil conditions.

2 Material and Methods

2.1 Plant Growth Conditions and Experimental Setup

Two soils with contrasting textures, sandy (S) and loamy (L), were selected to establish four treatments that combined soil texture and moisture conditions. Moisture conditions included well-watered (W) and water-limited (D) treatments. The loamy soil had a particle-size distribution of 33.2% sand, 47.7% silt, and 19.1% clay. The sandy soil was produced by mixing loamy soil with quartz sand at a 1:5 volume ratio, resulting in a final particle-size distribution of 88.6% sand, 8.1% silt, and 3.3% clay (Vetterlein et al., 2021). Before packing, soils were air-dried at 60°C, sieved to less than 2 mm, homogenized, and pre-treated with a nutrient solution as described by Vetterlein et al. (2021) to standardize nutrient availability across soil textures.

Maize (*Zea mays* L.) plants of the wild-type genotype B73 were cultivated in custom-designed aluminum rhizoboxes (internal dimensions: 40 cm × 42 cm × 1 cm; height × width × thickness). Rhizoboxes were packed horizontally to prevent visible layering during soil filling. Soil was added from the open top while continuously sieving through a 2 mm mesh to maintain uniform texture and avoid stratification. To establish gravel barrier regions (grain size 2.0–2.5 mm) at 10 cm intervals, a PVC frame (1 × 1 × 40 cm) was placed at each barrier location to create a temporary void. Soil was then sieved into the box and lightly rewetted by spraying from above to promote settling and consolidation. After packing the surrounding soil, the PVC frame was removed, and the void was filled uniformly with coarse gravel. This procedure resulted in a consistent bulk density of 1.4 g cm^{-3} in the L treatments and 1.6 g cm^{-3} in the S treatments. The top of each container was sealed with tape to prevent evaporative loss, enabling changes in soil water content to be referenced to plant transpiration.

The gravel layers functioned as capillary barriers, restricting the vertical movement of the D2O tracer after injection while permitting root growth. Unlike previous studies that used fully enclosed capillary barriers, which led to uneven soil moisture distribution and inadequate equilibration of soil water potential (Ahmed et al. 2016, 2018; Zarebanadkouki et al. 2012, 2013), the capillary barriers in this study were truncated by more than 1 cm on both lateral sides. This design enabled equilibration of water potential across compartments during plant growth and facilitated rapid re-equilibration after tracer injection, while minimizing the risk of cross-compartment tracer migration.

After packing, the volumetric soil water content of each treatment was adjusted to target values corresponding to the intended matric potentials (Table 1) and maintained by periodic gravimetric adjustment with tap water throughout the plant growth period. For loam, L-W and L-D treatments corresponded to water contents of 33–36% and 18–21%, respectively. For sand, S-W and S-D conditions were set at 18–21% and 6–10%, respectively. These values were selected to achieve comparable hydraulic conductivities in contrasting soil textures (Table 1).

Table 1: Volumetric water content (θ_{vol}, matric potential (h), and hydraulic conductivity (K) values for the four soil treatments. L: Loam, S: Sand, W: well-watered, D: water-limited

	W			**D**		
	θ_{vol} [%]	**h [hPa]**	**K [cm day^{-1}]**	**θ_{vol} [%]**	**h [hPa]**	**K [cm day^{-1}]**
L	33-36	-57.03	5.1	18-21	-544.74	6.3×10^{-3}
S	18-21	-38.08	13.7	6-9	-110.84	2.8×10^{-2}

Maize seeds were surface-sterilized in 10% H_2O_2 (v/v) for 10 minutes, rinsed with distilled water, soaked for 5 minutes, and then imbibed in a saturated $CaSO_4$ solution (0.015 M) for 3 hours. At a depth of 1 cm, maize seeds were sown and cultivated under controlled environmental conditions: a 12-hour photoperiod, temperatures of 22°C/18°C (day/night), 65% relative humidity, and photosynthetically active radiation at 350 µmol m^{-2} s^{-1}. After 45 days, neutron radiography was performed to visualize root water-uptake dynamics using D_2O as a tracer.

2.2 Neutron Radiography in Combination with D_2O Labelling

Neutron radiography was conducted at the NEUTRA and ICON beamlines of the Paul Scherrer Institute (Villigen, Switzerland). Images were acquired using an Andor iKon-L camera with a 63 µm pixel size and a spatial resolution of approximately 90 µm. Each image consisted of 2048 × 2048 pixels, providing a field of view of approximately 12 × 12 cm. Samples were exposed to the neutron beam for 20 seconds prior to image acquisition. D_2O served as a tracer to quantify in *situ root* water uptake along selected individual roots, following established protocols (Zarebanadkouki et al. 2012, 2013). Owing to its lower neutron attenuation coefficient relative to H_2O, D_2O facilitates visualization of water flow into roots using neutron radiography (Fig. 1 b). Before tracer application, a comprehensive radiographic scan of the container was performed to evaluate initial soil water distribution and root architecture. As the container exceeded the neutron camera's field of view, 12 overlapping radiographs were collected, normalized, and stitched together to reconstruct the complete sample (Fig. 1 a). The number of seminal and crown roots was determined, and the lengths of each root type were measured from the radiographic images.

https://doi.org/10.5194/egusphere-2026-1740
Preprint. Discussion started: 29 April 2026

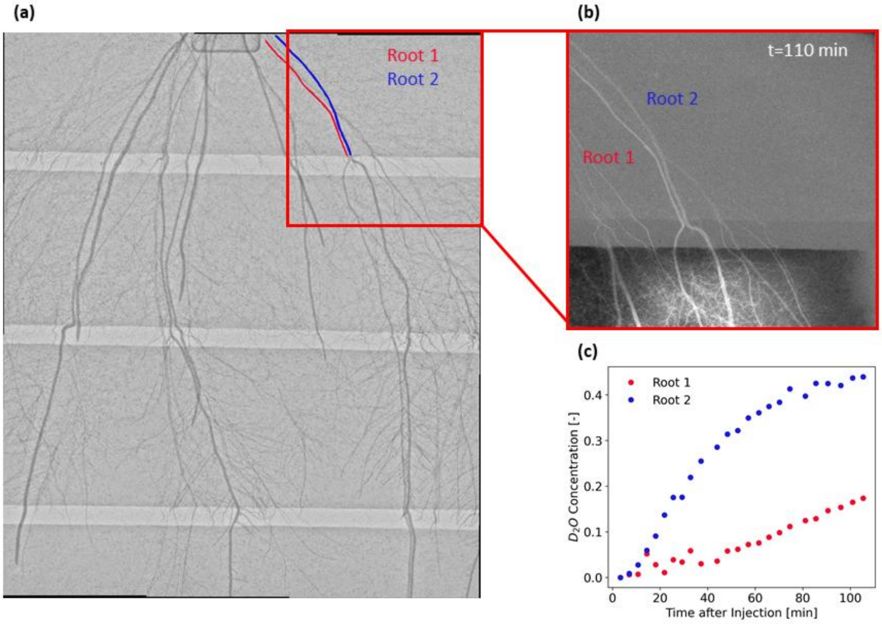

Figure 1: (a) Neutron radiograph of an exemplary root system. Full scan was compiled by stitching 12 images with the field of view of 12 x 12 cm. Neutron radiography is sensitive to water, the darker the image, the higher the water content. Brighter lines are the capillary barriers of a different grain size. In red and blue are two exemplary roots segmented. (b) is the difference image after 110 minutes after injection divided by the first image, before injection. D_2O uptake appears as brighter objects. Based on the change in contrast, the D_2O concentration can be calculated, as shown in (c). The D_2O concentration over time, as a mean of the total root segment.

A volume of approximately 75 mL of D_2O was injected into each soil compartment at two positions using a fine syringe, resulting in a localized increase in volumetric water content of approximately 4.5%. After injection, the spatiotemporal dynamics of D_2O transport were monitored using time-series neutron radiography with a temporal resolution of 20 seconds over approximately 2 hours (Fig. 1 b). Once tracer uptake and transport within the roots had ceased, the procedure was repeated in the next upper compartment. Conducting the labelling experiment in two to three compartments enabled spatially resolved quantification of root water uptake and axial water transport along individual root segments.

The D_2O labelling experiment was conducted both at night and during periods during the day. The nighttime experiment aimed to quantify the diffusion coefficient of root tissue in the absence of transpiration between 18:00 and 04:00. During this period, plant shoots were sealed in an opaque plastic

https://doi.org/10.5194/egusphere-2026-1740
Preprint. Discussion started: 29 April 2026

bag for 4 hours prior to measurements to minimize transpiration. For daytime experiments, a LED growth light (GC 9, Greenception GmbH, Hamburg, Germany) was installed in the beamline to quantify actual root water uptake rates. Before the labelling experiment, plants were illuminated with the LED growth light for 1 hour to simulate daytime conditions. Under these conditions, maize grown in well-watered sandy soil exhibited an average transpiration rate of approximately 7.3 g h^{-1}, while under water-deficient sandy conditions, the rate was approximately 0.9 g h^{-1}. Maize grown in loamy soil transpired at rates of 10.2 g h^{-1} and 2.8 g h^{-1} under L-W and L-D conditions, respectively.

2.3 Image Processing of Neutron Radiographs and D_2O Concentration

Neutron radiographs were processed to determine the temporal evolution of D_2O concentration within individual root segments. Image processing followed the established workflow described in Zarebanadkouki et al. (2012, 2013). In summary, each raw radiograph was corrected for dark current (signal recorded by the camera in the absence of the neutron beam) and normalized using a corresponding open beam image (signal recorded in the absence of any sample in front of the beam prior to each labelling experiment) to eliminate spatial illumination heterogeneity. The normalized intensity at each pixel was converted to D_2O concentration using the Beer–Lambert law, applying the specific neutron attenuation coefficients of H_2O, D_2O, and dry soils determined for the NEUTRA and ICON beamlines. Owing to the strong contrast between roots and surrounding soil, selected root regions above the capillary barrier were visually segmented from the image acquired before D_2O injection. The segmented masks were used to calculate D_2O concentrations at each time frame and were averaged across the root tissue in the radial direction to generate concentration-time profiles along each analyzed root segment at a specified distance from the root tip (Adamczewski and Zarebanadkouki, 2026).

2.4 Modelling Root Water Uptake Using D_2O Concentration Dynamics

Local root water uptake (RWU) was quantified by analyzing the spatiotemporal propagation of D_2O within the root system. A semi-two-dimensional diffusion–convection model was developed to describe the spatiotemporal transport of D_2O within root segments situated above the capillary barrier. The theoretical foundation was based on the conceptual framework of Zarebanadkouki et al. (2012, 2013), with numerical implementation and parameter estimation tailored to the objectives of this study. Following D_2O injection into a soil compartment, the labelled water entered the root and moved radially across root tissues through both molecular diffusion and radial root water uptake (advective transport) (Fig. 2). Upon reaching the xylem, the tracer was transported upward along the root by axial water flow. The analysis focused on the evolution of D_2O concentration within the root segment above the capillary barrier. In this segment, D_2O was transported axially by a combination of advection and diffusion, while simultaneously diffusing radially from the xylem into the surrounding root tissues. This radial diffusion was counteracted by the continuous inflow of non-labelled water from the surrounding soil, which diluted the tracer concentration within the root tissues (Fig. 2).

https://doi.org/10.5194/egusphere-2026-1740
Preprint. Discussion started: 29 April 2026

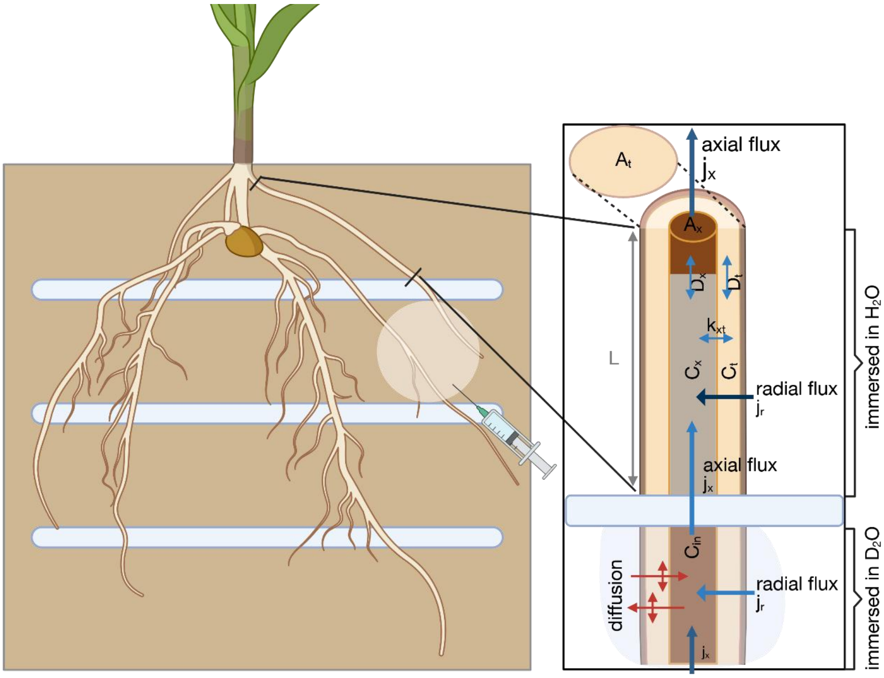

Figure 2: (a) Schematic of a maize plant growing in the rhizobox, labelled with D_2O in the second compartment. (b) The basic concept underlying the model is presented. D_2O is taken up below the capillary barrier by a radial flux (j_r) into the root and diffusion. Subsequently this tracer moves upwards in the xylem by the axial flux (j_x). By active water uptake (j_r) and outwards diffusion the tracer signal will be attenuated. The figure was created in BioRender: Adamczewski, R. (2026), https://BioRender.com/50hev05

A simplified representation of D_2O transport within the analyzed root segment was achieved by modeling the root cross-section as two distinct radial compartments: (i) the xylem domain, where axial transport dominated and the tracer concentration was denoted by $C_x(z,t)$, and (ii) the surrounding root tissue domain, where tracer exchanged radially with both the xylem and the surrounding soil, with concentration $C_t(z,t)$. The cross-sectional areas of these two compartments were denoted by A_x and A_t, respectively. This framework is conceptualized in Fig. 2b.

Applying conservation of tracer mass to the xylem compartment yielded

$$\frac{\partial C_x}{\partial t} = -\frac{\partial}{\partial z}(j_x C_x) + D_x \frac{\partial^2 C_x}{\partial z^2} + \frac{k_{xt}}{A_x}(C_t - C_x) \tag{1}$$

where $j_x(z)$ is the axial water flux within the xylem [$\mathrm{cm\,s^{-1}}$], D_x is the effective axial diffusion coefficient within the xylem domain [$\mathrm{cm^2\,s^{-1}}$], and k_{xt} represents the exchange rate of tracer between

https://doi.org/10.5194/egusphere-2026-1740
Preprint. Discussion started: 29 April 2026

the root tissues and the xylem. The first term on the right-hand side describes advective transport of tracer along the root axis, the second term represents axial diffusion, and the third term accounts for exchange of tracer between the two root compartments.

The corresponding tracer mass balance for the surrounding root tissues is

$$\frac{\partial C_t}{\partial t} = D_t \frac{\partial^2 C_t}{\partial z^2} + \frac{2\pi r j_r}{A_t}(C_{in}(t) - C_t) + \frac{k_{xt}}{A_t}(C_x - C_t) \tag{2}$$

where D_t is the effective diffusion coefficient in the root tissue domain [$\mathrm{cm}^2\ \mathrm{s}^{-1}$], r is the root radius [cm], and j_r represents the radial influx of water per unit root surface area [$\mathrm{cm\ s}^{-1}$]. The term $2\pi r j_r(C_{in} - C_t)$ describes the entry of labelled water from the surrounding soil into the root tissues, where $C_{in}(t)$ denotes the tracer concentration in the water entering the root. For root segments located above the capillary barrier, this concentration was assumed to be zero because the surrounding soil remained unlabelled during the experiment. Exchange between root tissues and the xylem is represented by the terms containing k_{xt}, which drives equilibration between the two compartments.

Under the assumption of incompressible flow and constant water content within the root, the spatial variation of axial xylem flow is governed by the continuity equation

$$\frac{\partial(\pi r_x^2 j_x)}{\partial z} = 2\pi r j_r \tag{3}$$

where r_x is the radius of the xylem and r is the radius of the root. For simplicity, $r_x$was assumed constant along the analysed root segment. This relation implies that axial xylem flux increases with distance from the distal end of the analysed root segment toward the root base as water is taken up radially along the root. Once the radial uptake rate is specified, this equation uniquely determines the axial flow profile along the analysed root segment.

Because neutron radiography measures the average tracer concentration across the full root thickness, simulated tracer concentrations were calculated as the cross-sectional average concentration of the two compartments

$$C_{sim}(z,t) = \frac{A_x C_x(z,t) + A_t C_t(z,t)}{A_x + A_t} \tag{4}$$

This averaging step ensures that simulated tracer concentrations correspond directly to the experimentally observed signal.

2.5 Parameterization and Numerical Solution of the Transport Model

The governing equations (Eq. 1 and 2) were solved numerically in Python using a finite-difference scheme on the domain $0 \le z \le L$, where L is the length of the analyzed root segment [cm]. This domain corresponds to the segmented root portion located above the capillary barrier. The root segment was discretized into n_z nodes with uniform spacing. For each analyzed root segment, the mean root radius was determined from the segmented root mask obtained from neutron radiographs. The total root cross-sectional area was then calculated as $A_{tot} = \pi r^2$. This area was partitioned into a xylem domain and a surrounding tissue domain. The xylem area A_x was assumed to represent 5% of the total root cross-section, while the remaining area was assigned to the tissue compartment as $A_t = A_{tot} - A_x$. Effective diffusion coefficients describing axial spreading of the tracer within the root were determined independently from nighttime tracer experiments, during which transpiration-driven flow was minimized. Under these conditions, radial transport of D_2O within root segments immersed in D_2O was inversely solved using a diffusion model following the workflow developed by Zarebanadkouki et al. (2013, 2014). The resulting diffusion coefficients were subsequently used as fixed parameters in the transport simulations.

The governing equations were subjected to zero tracer concentration as initial conditions,

$$\begin{aligned} C_x(z,0) &= 0 \\ C_t(z,0) &= 0 \end{aligned} \tag{5}$$

representing tracer-free root tissues prior to the arrival of the D_2O front. The model was further subjected to the following boundary conditions. At the upper boundary of the analyzed segment ($z = L$), zero-gradient conditions were imposed for both compartments,

$$\frac{\partial C_x}{\partial z} = 0, \frac{\partial C_t}{\partial z} = 0 \tag{6}$$

representing free continuation of tracer transport beyond the analyzed region. At the root surface, radial influx of water was prescribed through the radial flux j_r. Because the surrounding soil above the capillary barrier remained unlabeled during the experiment, the tracer concentration associated with this radial influx was assumed to be zero. At the lower boundary of the analyzed root segment ($z = 0$), the model was subjected to a prescribed axial inflow $j_x(z = 0)$ representing the upward transport of labelled water from the soil compartment below the capillary barrier. In principle, this boundary condition requires knowledge of the tracer concentration entering the analyzed segment through the xylem. However, this concentration cannot be directly measured. To overcome this limitation, simulations were initiated at the moment when the D_2O front reached the analyzed root domain. In practice, we began the simulations at the first root segment located immediately above the D_2O/H_2O front and used only segments located at least 2 cm above this point. This typically corresponded to initiating the simulations approximately 4-8 minutes after tracer injection began. Under this condition, it is reasonable to assume that the tracer concentration entering the analysis segment through the xylem had already equilibrated with the D_2O concentration in the injected soil compartment. The initial tissue concentration at the lower boundary was therefore calculated from the measured average concentration C_{tot} using the cross-sectional averaging relation described above.

2.6 Inverse Modelling

The unknown model parameters estimated by inverse modelling were the axial inlet flux $j_x(z=0)$, the spatial variation of radial water uptake $j_r(z)$ along the analysed root segment, and the exchange coefficient k_{xt} between xylem and root tissue. To facilitate inverse modelling and to avoid fitting an independent radial uptake value at each node, we assumed that the axial xylem flux profile along the analysed root segment can be described by a simple parametric function,

$$j_x(z) = j_{x,0}\,(1+az)^b \tag{7}$$

where $j_{x,0}$ is the axial xylem flux at the lower boundary of the analysed segment ($j_x(z=0)$), and a and b are empirical shape parameters controlling the magnitude and axial variation of xylem flow along the root. Note that a and b were let to be chosen positive or negative ensuring a constant, increasing, or decreasing profile of $j_x(z)$ with distance from the root distal part. Under the assumption of a constant xylem radius r_x, the radial water uptake profile was then calculated from the continuity equation as

$$j_r(z) = \frac{1}{2\pi r}\frac{\partial(\pi r_x^2 j_x)}{\partial z} \tag{8}$$

which simplifies to

$$j_r(z) = \frac{r_x^2}{2r}\frac{\partial j_x}{\partial z} \tag{9}$$

This formulation ensures that radial uptake and axial flow remain physically consistent, while reducing the dimensionality of the inverse problem.

These parameters were estimated using the D_2O concentration profiles derived from neutron radiographs. For each analysed root segment, the experimental data consisted of tracer concentration as a function of time and axial position along the root. These data were extracted from the segmented root region and averaged across the radial direction to obtain the measured concentration field.

By minimizing the difference between simulated and measured tracer concentrations, the model parameters were determined. The objective function was formulated as the sum of squared residuals between observation and simulation across all spatial nodes and time steps,

$$\Phi = \sum_{i=1}^{Nz}\sum_{j=1}^{N_t}\left[C_{\text{obs}}(z_i,t_j) - C_{\text{sim}}(z_i,t_j)\right]^2 \tag{10}$$

where C_{obs} denotes the concentration obtained from neutron radiography and C_{sim} represents the simulated concentration, z_i refers to the root segment and t_j refers to a measured time.

Parameter estimation was carried out using a multistart optimization procedure implemented in Python. Initial parameter sets were sampled within physiologically plausible ranges, and each set was subsequently refined using a local nonlinear optimization algorithm until convergence was achieved. The parameter set that minimized the objective function was selected as the optimal solution for the analyzed root segment. The exact procedure of numerical modelling is detailed in the script uploaded at GitHub (Adamczewski and Zarebanadkouki, 2026)

2.7 Statistical Analysis

To obtain if treatments led to statistically different results, a two-way analysis of variance (ANOVA) implemented in Python using the statsmodels.stats package (Perktold et al., 2024) was conducted. Before ANOVA was calculated, data were assessed for normality and homogeneity of variance in the residuals using the scipy.stats package (Virtanen et al., 2020). If the residuals of the data were not normal distributed or homogeneous distributed, data was log or Box-Cox transformed. If statistical significances occurred a post-hoc Tuckey test was performed.

3 Results

3.1 Plant Growth and Transpiration Response to Soil Texture and Moisture

Soil texture and moisture strongly influenced maize growth and transpiration. After six weeks of cultivation, plants grown under well-watered conditions reached comparable heights in both soils, with mean values of 57 ± 2 cm in S–W and 57 ± 6 cm in L–W. Under water-limited conditions, plant height was significantly reduced, particularly in sand: S–D plants reached 36 ± 5 cm, whereas L–D plants attained 47 ± 4 cm, indicating that drought stress was more restrictive in the sandy soil (Table 2). A two-way ANOVA confirmed that plant height was significantly affected by soil moisture availability ($p < 0.001$), with a significant interaction between soil texture and water availability ($p < 0.01$).

Transpiration rates measured one day prior to the experiment followed a similar pattern (Table 2), and in addition showed a direct influence of soil texture ($p < 0.001$). The highest transpiration rate was observed in L-W (22 ± 5 g day^{-1}), followed by S-W (18 ± 1 g day^{-1}). Plants grown in L-D transpired approximately 16 ± 3 g day^{-1}, which was significantly lower than in L-W conditions, but not significantly different from the S-W. The significantly lowest transpiration rate was recorded in S-D, with an average of 7 ± 2 g day^{-1}.

Table 2: Height of 45-day-old maize plants grown under contrasting soil texture and moisture conditions, measured immediately before imaging and daily transpiration rate measured one day prior to tracer application. Statistical significance from ANOVA is reported in the text; different letters denote significant differences among treatments (Tukey, $p < 0.05$). Treatments: L = loam, S = sand, W = well-watered, D = water-limited.

	L		**S**	
	W	**D**	**W**	**D**

Plant height [cm]	57 ± 6 ^{a}	47 ± 4 ^{b}	57 ± 2 ^{a}	36 ± 5 ^{c}
Transpiration [g day^{-1}]	22 ± 5 ^{ac}	16 ± 3 ^{bc}	18 ± 1 ^{c}	7 ± 2 ^{d}

3.2 Root Number and Root Length and Root Radius Development in Response to Soil Texture and Moisture

Belowground responses revealed that maize root system architecture was modulated by soil texture and moisture availability. The total number of CR was not significantly affected by soil treatment; nevertheless, plants grown in sandy soil tended to produce slightly more CR (S–W: 11 ± 2.2; S–D: 8.4 ± 1.8) than those in loamy soil (L–W: 7.4 ± 2.4; L–D: 8.6 ± 2.6; Fig. 3a). A comparable pattern was observed for SR, with marginally higher numbers in S relative to L (S–W: 4.5 ± 0.6; S–D: 4.4 ± 1.5; L–W: 3.6 ± 0.5; L–D: 4 ± 0.7; Fig. 3b).

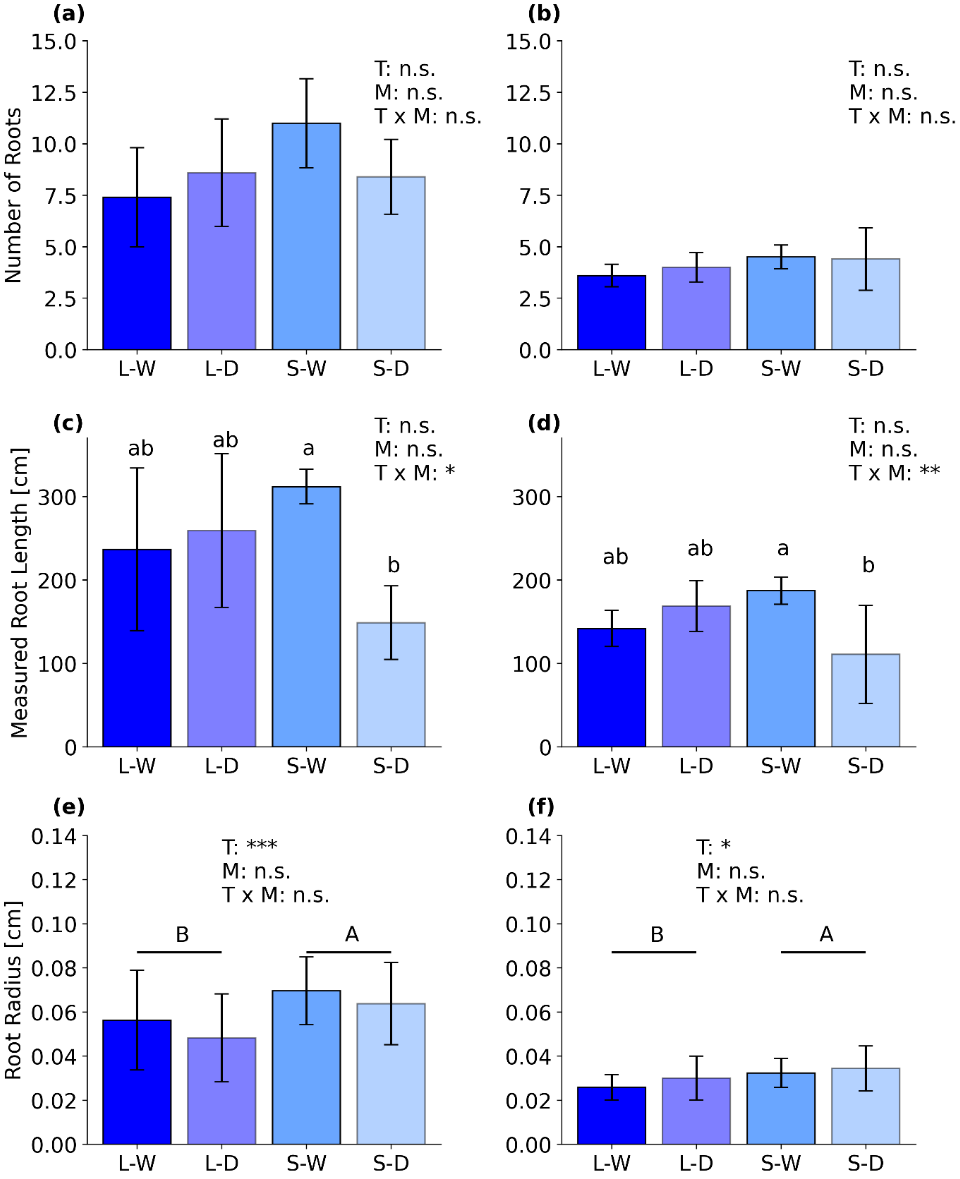

*Figure 3: (a, b) Number of crown roots (CR, a) and seminal roots (SR, b) quantified from the full scan neutron radiograph obtained on the day of experiments. (c, d) Root length (cm) of CR (c) and SR (d) measured from the full scan neutron radiograph. (e, f) Root radius of segmented CR (e) and SR (f) used in RWU analysis. Bars represent means, and error bars indicate standard deviation across six replicates per treatment. The two-way ANOVA results are provided in the text ($p < 0.001$ = ***, $p <$*

*0.01 = **, $p < 0.05$ = *). Post-hoc Tukey test results are indicated by letters ($p < 0.05$).* ***Abbreviations****: L, loam; S, sand; W, well-watered; D, water-limited; T, texture; M, moisture.*

In contrast to root number, CR and SR lengths were markedly influenced by the interaction between soil texture and moisture regime. In sandy soil, total CR length was significantly greater under well-watered conditions (S–W: 312 ± 20.7 cm) than under drought (S–D: 149 ± 44 cm), whereas CR length in loamy soil did not differ significantly between moisture treatments (Fig. 3c). SR followed a similar pattern: roots were substantially longer in S–W (187.5 ± 16.4 cm) compared with S–D (111 ± 59.7 cm), while no significant moisture-driven differences were detected in loamy soil (Fig. 3d).

Root radius was significantly influenced by soil texture for both CR and SR. In both cases, roots developed in S exhibited a significantly larger radius compared to those in L (CR: 0.067 ± 0.017 cm in S vs. 0.052 ± 0.022 cm in L; SR: 0.034 ± 0.009 cm in S vs. 0.028 ± 0.008 cm in L; Fig. 3e, f). The root radius of CR tended to be slightly greater under W conditions compared to D, whereas SR displayed the opposite trend, with a marginally larger radius under drought. Overall, root radius was primarily determined by soil texture, with a more subtle, root type-specific response to soil moisture.

3.3 Image-Based Visualization of D_2O Transport

Figure 1a presents an exemplary neutron radiograph showing the root distribution of a sample (S-D) prior to D_2O injection. The color intensity in the image reflects water content, with darker areas corresponding to higher water content. The soil water distribution was homogeneous at 18% throughout the entire sample, as indicated by the uniform grey value across all compartments. This uniform distribution corresponds to a matric potential of -36 cm, as determined from the soil water retention curve (Vetterlein et al., 2021). The capillary barriers can be seen in brighter grey values, as the attenuation coefficient of the gravel-filled regions was lower than that of the rest of the soil (due to low water contents).

By dividing the initial image from subsequent images taken after D_2O injection, D_2O transport can be visualized and quantified, owing to its lower attenuation coefficient. Figure 1b displays the resulting difference image between t_0 and $t = 110$ min. Root segments above the capillary barrier appear brighter where D_2O uptake and transport have occurred. The increase in D_2O concentration over time in the segmented roots, highlighted in red and blue in Figure 1a and located above the capillary barrier, is shown in Figure 1c. Following injection, D_2O concentrations increased exponentially until reaching a plateau, indicating equilibrium between H_2O and D_2O.

3.4 Diffusivity of Maize Roots under Contrasting Soil Conditions

The average diffusion coefficient across all maize root segments was $1.1 \pm 2.1\times10^{-7}$ cm^2 s^{-1}. Root tips (0–7 cm from apex) exhibited higher mean diffusivity ($1.2 \pm 1.5\times10^{-7}$ cm^2 s^{-1}), whereas mature root segments (15-40 cm from tip) showed a slightly lower diffusivity (1.1 ± 2.5×10^{-7} cm^2 s^{-1}, Fig. 4), although this difference was not statistically significant. For root tips, soil texture influenced the apparent diffusion coefficient of roots, with higher diffusion coefficients in S and lower in L ($p < 0.01$; Fig. 4a). The diffusion coefficient of S was 1.9 ± 2×10^{-7} cm^2 s^{-1}, while in L it was 4.6 ± 2.6×10^{-8} cm^2 s^{-1}. The ANOVA revealed an impact of soil moisture on the diffusivity of roots in mature parts of the roots ($p < 0.05$; Fig. 4b). Roots were less permeable in maize plants grown under D conditions (4.5 ± 2.6×10^{-8} cm^2 s^{-1}) compared to maize plants grown under W conditions (1.8 ± 3.5×10^{-7} cm^2 s^{-1}).

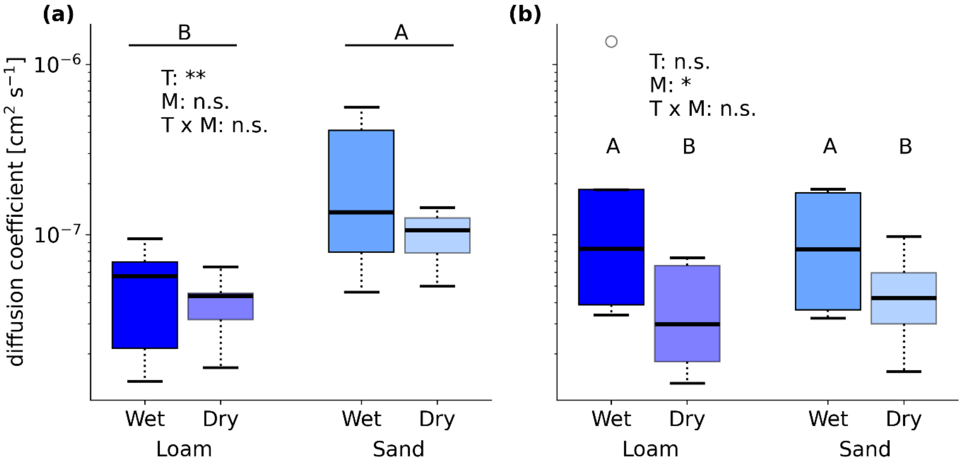

*Figure 4: (a) Diffusion coefficients (D) of root tips (0–5 cm from the root tip). (b) Diffusion coefficients (D) of mature root segments (>15 cm from the root tip). The two-way ANOVA results are presented in the text ($p < 0.001$ = ***, $p < 0.01$ = **, $p < 0.05$ = *). The post-hoc Tukey test identified significantly higher D in sandy soil (S) for CR ($p < 0.05$) and significantly higher D under well-watered (W) conditions for SR.* ***Abbreviations****: T, texture; M, moisture.*

In each boxplot, the box spans the interquartile range (25th to 75th percentile) with the median indicated by a black horizontal line. The whiskers reach the most extreme values within 1.5 × IQR, while observations beyond this range are shown as fliers (outliers).

3.5 Root Water Uptake of Maize Under Contrasting Soil Conditions Among Different Roots

D_2O-labelling experiments combined with inverse modelling revealed clear differences in RWU between root types and soil treatments calculated for the root segments located at 7–13 cm from the plant collar. Soil texture significantly affected the radial flux (j_r) of CR, with RWU being 3.3 times higher in sandy soil than in loamy soil (2.4 ± 0.7 × 10^{-3} cm min^{-1} in S vs. 7.5 ± 5.7 × 10^{-4} cm min^{-1} in L; Fig. 5a). Soil moisture exerted only a weak influence ($p < 0.1$), with slightly higher radial fluxes observed under dry conditions compared with wet soils. In contrast, RWU of SR showed no significant response to any treatment, although a weak trend suggested 1.3-fold higher uptake rates in sandy compared with loamy soils ($8.6 \pm 4.2 \times 10^{-4}$ cm min^{-1} in S vs. $6.7 \pm 3.6 \times 10^{-4}$ cm min^{-1} in L; Fig. 5b).

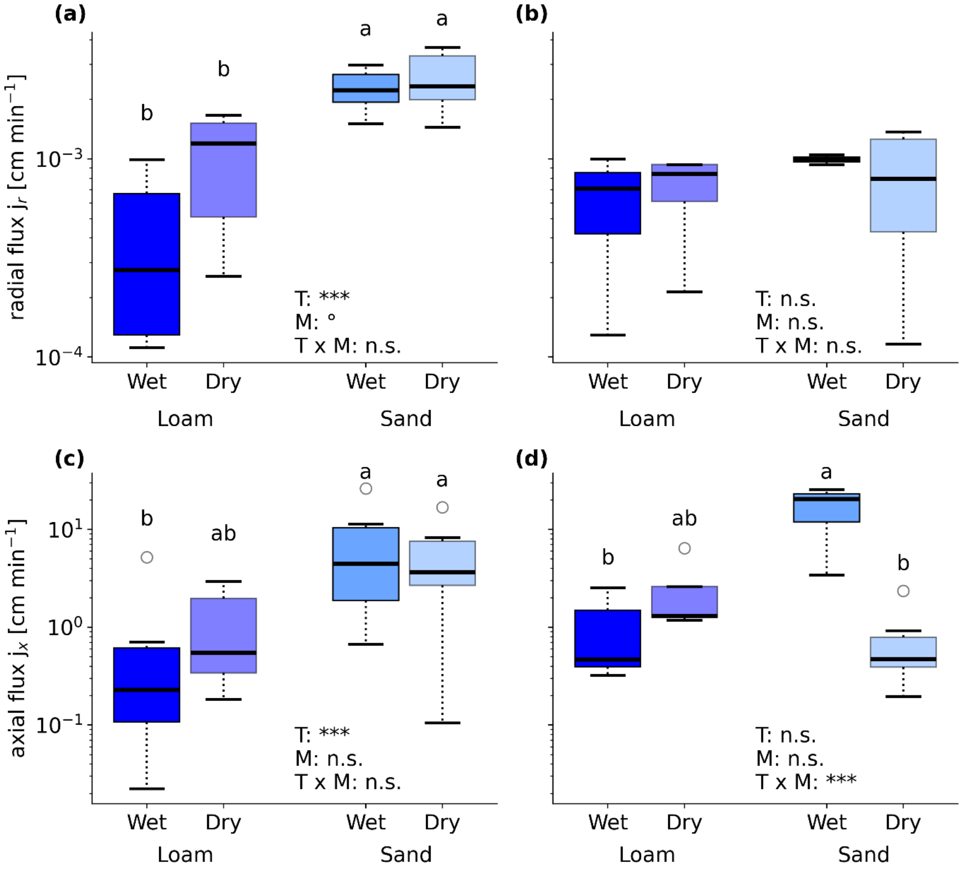

*Figure 5: Boxplots of the fitted radial flux j_r [cm min^{-1}] (a, b), fitted axial flux j_x [cm min^{-1}] (c, d) obtained for the root segments located at 7-13 cm from the plant collar. Left column (a, c) shows results for CR and the right column (b, d, f) for SR. ANOVA results are presented ($p < 0.001$ = ***, $p < 0.01$ = **, $p < 0.05$ = *, $p < 0.1$ = °). The results of the post-hoc Tukey test ($p<0.05$) are denoted by different letters.* ***Abbreviations****: T, texture; M, moisture.*

Axial fluxes (j_x) in CR calculated for the root segments located at 7–13 cm from the plant collar were also significantly influenced by soil texture, resulting in a 5.7-fold higher axial flux in sandy soil (6.5 ± 6.9 cm min^{-1}) compared with loamy soil (1.1 ± 1.5 cm min^{-1}; Fig. 5c). For SR, axial fluxes were affected by the interaction between soil texture and soil moisture, with similar values observed in L-W and S-D, slightly higher fluxes in L-D, and the highest fluxes in S-W (Fig. 5d). It should be noted that SR possess a smaller xylem cross-section than CR, which is reflected in an approximately two-fold smaller root radius (Fig. 3e, f), implying greater volumetric flow in CR than in SR.

4 Discussion

4.1 Soil Texture Exerted a Stronger Control on Crown Root Uptake Than Soil Moisture

The present study demonstrates that soil texture exerts a substantially stronger influence on radial water uptake (j_r) and axial transport (j_x) in crown roots (CR) than soil moisture (Fig. 5a, c; Fig. 6). Radial fluxes in CR were approximately three times increased in sandy than in loamy soil, whereas differences between wet and dry conditions within each soil were comparatively small. This indicates that crown root water uptake responded primarily to soil texture rather than to the imposed moisture regimes. In contrast, seminal roots (SR) exhibited a much more consistent uptake pattern across soil textures and moisture treatments. Their radial fluxes varied only moderately among treatments, suggesting that SR hydraulic functioning was less sensitive to variations in the surrounding soil environment.

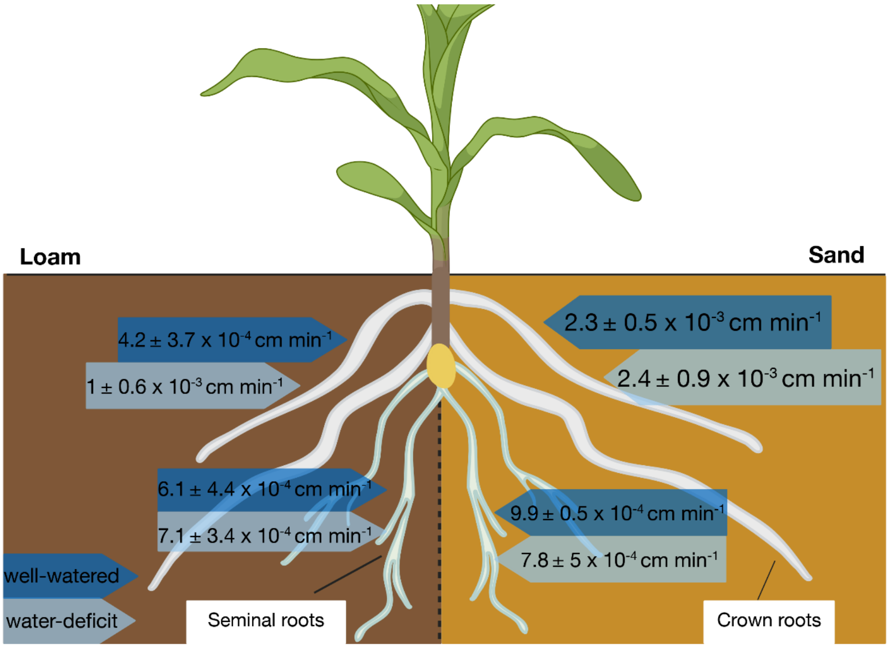

Figure 6: Summary of obtained radial fluxes in contrasting soil conditions. Dark-blue colored arrows show results of well-watered treatments, light-blue colored arrows of water-deficit treatments. The figure was created in BioRender: Adamczewski, R. (2026) *https://BioRender.com/3lg4kkf*

https://doi.org/10.5194/egusphere-2026-1740
Preprint. Discussion started: 29 April 2026

The strong texture effect observed for CR cannot be explained solely by soil matric potential or by the bulk soil's hydraulic conductivity. Classical soil–plant hydraulic theory predicts that root water uptake scales with both soil hydraulic conductivity and the water potential gradient between the soil and the root (Passioura, 1988; Steudle, 1994). Under this framework, radial uptake is expected to be highest in wet loamy soil, where hydraulic conductivity is typically greater than in dry sandy soil (Table 1). However, our results showed the opposite pattern: radial fluxes in sandy soil exceeded those in loamy soil under both moisture regimes, and even dry sand supported higher j_r than wet loam (Fig. 5a). This indicates that bulk soil hydraulic conductivity alone did not control water uptake in our system.

Instead, water flow from soil to xylem is governed by a sequence of hydraulic resistances, including the bulk soil, the rhizosphere, and the root tissues themselves. In such a system, local radial water fluxes are not determined solely by soil hydraulic properties but also by the root system's hydraulic architecture, which shapes the distribution of xylem water potential along the root axis (Landsberg and Fowkes, 1978; Steudle and Frensch, 1989). This potential profile depends on the balance between radial hydraulic conductivity of the root and axial conductance of the xylem (Zwieniecki et al. 2002), as well as the overall hydraulic conductance at the plant collar. Consequently, even when soil hydraulic conditions are similar, differences in axial and radial root conductance can generate substantially different radial flux patterns along roots. In this context, the higher j_r observed for crown roots in sandy soil suggests that maize roots growing in sand may operate with a more effective internal hydraulic architecture. Measurements of maize root hydraulics support this interpretation. For example, Meunier et al. (2018) showed that both axial conductance and radial hydraulic conductivity can vary strongly among maize root types and that conductance at the root–shoot junction can also contribute significantly to the overall hydraulic pathway. Such variation indicates that plant hydraulic regulation is distributed across several components of the root system rather than being fixed. Differences in axial conductance or collar conductance could therefore alter the xylem water potential profile along crown roots and ultimately increase the driving force for radial water uptake.

Finally, hydraulic conductance at the root–soil interface may also have played an important role. The rhizosphere forms the immediate hydraulic connection between roots and soil and can strongly modify water flow toward roots. Recent work on maize grown in the same sand–loam system showed that crown roots developed a more pronounced and wetter rhizosphere in sandy soil, with greater rhizosphere extension and higher water content at the root–soil interface (Adamczewski et al., 2025). Such rhizosphere development can increase hydraulic continuity between soil and root and reduce resistance at the root–soil interface. In contrast, weaker rhizosphere development in loam could lead to lower hydraulic connectivity and therefore reduce radial water uptake. These observations are consistent with our finding that crown roots exhibited substantially higher j_r in sand but only minor responses to moisture variations within each texture.

https://doi.org/10.5194/egusphere-2026-1740
Preprint. Discussion started: 29 April 2026

4.2 Crown and Seminal Roots Exhibited Contrasting Hydraulic Behavior

A second major finding of this study was the clear hydraulic differentiation between crown roots and seminal roots. Across most treatments, radial uptake rates of SR were consistently lower than those of CR, except in wet loam where uptake rates were similar. On average, radial uptake of CR exceeded that of SR by approximately 2-fold, indicating that crown roots contributed substantially more to water uptake under the investigated conditions (Fig. 5a, b). From a plant perspective, the volumetric flow associated with a unit length of root can be estimated as $Q = 2\pi r j_r$, where r is the root radius. Because crown roots in our study had approximately twice the radius of seminal roots and exhibited two times higher radial fluxes, the resulting volumetric flow per unit root length can be expected to be 4 times larger in CR. When these effects are combined, a single centimeter of crown root is likely to transport four-times more water than an equivalent length of seminal root, highlighting the disproportionate contribution of CR to whole-plant water uptake.

These findings align with previous studies, showing anatomical and hydraulic differences between maize root types. Crown roots typically possess larger xylem vessels and greater xylem cross-sectional area than seminal roots, resulting in higher axial conductance (Hazman and Kabil, 2022). Because axial hydraulic conductance scales with the fourth power of vessel radius, even modest increases in vessel diameter can produce substantial gains in hydraulic capacity (Poorter et al., 2010). Experimental measurements have also shown that radial hydraulic conductivity can differ between root types, reflecting differences in anatomy and development of apoplastic barriers (Meunier et al., 2018). Imaging studies of maize roots further demonstrate that the contribution of seminal roots to plant water uptake declines as crown roots develop and become hydraulically dominant (Ahmed et al. 2016; 2018).

4.3 Root System Architecture Amplified Hydraulic Differences

Hydraulic differences between root types were further reinforced by differences in root system architecture. Crown roots were more numerous and contributed substantially more to total root length than seminal roots. Consequently, crown roots provided a larger absorbing surface area for water uptake. This architectural advantage amplified the hydraulic importance of CR. Even if radial uptake rates per unit root surface had been similar between root types, the greater number and length of CR would still result in a larger overall contribution to plant water uptake. In the present study, crown roots combined higher radial uptake rates, larger diameters, and greater total length, making them the dominant pathway for water acquisition across all tested soil conditions.

These observations are consistent with the concept of root hydraulic architecture, in which both root hydraulic properties and spatial arrangement determine water uptake patterns (Doussan et al., 2006). Roots that combine high radial permeability with large axial conductance and favorable architecture can dominate water uptake even when growing in similar soil environments (Zwieniecki et al. 2002). The higher axial fluxes observed in CR in the present study are therefore consistent with their greater cumulative radial uptake along the root axis.

4.4 Uncertainties of Model Assumptions to Axial Fluxes

The comparison of j_x across treatments should be interpreted with caution, as their numerical values are highly sensitive to assumptions regarding xylem cross-sectional area. In the present model, the conductive xylem fraction was assumed to be constant across all treatments. However, axial flow is directly proportional to the conductive area (i.e., $\propto \pi r_x^2$), meaning that even small deviations in the assumed xylem radius can lead to substantial differences in the estimated j_x. As a result, the absolute values of axial flux, as well as their comparison between treatments, may partly reflect modelling assumptions rather than true physiological differences.

This limitation becomes particularly relevant when comparing treatments such as L–W and L–D, as well as sandy versus loamy soils. In our results, j_x was consistently lower in the L–W treatment compared to L–D, and lower in loamy soil than in sandy soil. At the same time, plants in L–W exhibited higher transpiration rates (Table 2), while having fewer crown and seminal roots and a lower total root length (Fig. 3). Taken together, these observations would suggest that axial flux per root segment, especially in the uppermost compartments where j_x was evaluated, should be higher rather than lower. This apparent contradiction raises the question of how the higher transpiration demand was sustained if axial transport capacity, as estimated by the model, was lower.

One possible explanation is that the model underestimates axial flux due to uncertainties in xylem geometry. Because axial flow scales with the conductive xylem area, even small inaccuracies in the assumed xylem radius can substantially affect the estimated j_x. If the xylem fraction is overestimated for roots grown in loamy soil, the resulting j_x values will be underestimated. Conversely, if the xylem fraction is underestimated for roots grown in sandy soil, the fitted axial flux may be artificially elevated. Evidence from previous work suggests that such anatomical differences between soil treatments are plausible. Vetterlein et al. (2022) reported that maize roots grown in the same sandy and loamy soil system in the field show significant differences in internal anatomy, with a larger relative vascular bundle area in roots grown in loamy soil compared with sandy soil. These findings indicate that soil texture can influence xylem development and vascular proportions, which in turn affect axial hydraulic conductance. Consequently, assuming a constant xylem fraction across soil treatments likely introduces systematic uncertainty into model-derived estimates of axial flux. Therefore, the observed differences in j_x between treatments should be interpreted with caution, particularly when used to infer physiological differences in water transport.

5 Conclusion

This study provides direct quantification of radial and axial water fluxes along individual maize roots growing under contrasting soil conditions. The results demonstrate that soil texture exerted a stronger control than soil moisture on crown root uptake and that radial water uptake cannot be explained solely by bulk soil hydraulic conductivity. Instead, water uptake emerged from the interaction between soil-root hydraulic coupling, root-type-specific hydraulic properties, and root system architecture. Crown roots acted as the dominant and most plastic uptake pathway, whereas seminal roots maintained a more stable background uptake capacity. These findings emphasize the importance of considering root-type-specific hydraulic functioning and rhizosphere processes when analyzing plant water uptake and when developing mechanistic models of soil–plant water relations.

Supplementary Data

Code availability

The image processing and inverse modelling code is available on GitHub (Adamczewski and Zarebanadkouki, 2026).

Data availability

The datasets generated and/or analyzed in the present study are available from the corresponding authors upon reasonable request.

Author contributions

RA, AK, JP, MH, MZ contributed to the study conception and design. RA and MZ performed the material preparation, data collection, modelling, and analysis. RA, AK and MZ carried out experiments. RA wrote the first draft of the manuscript and all authors commented on previous versions of the manuscript. All authors read and approved the final manuscript.

Conflict of interest

The authors declare that they have no conflict of interest.

Acknowledgments

This work is based on experiments performed at the Swiss spallation neutron source SINQ, Paul Scherrer Institute, Villigen, Switzerland. Seeds of the maize wild type B73 were provided by Caroline Macron and Frank Hochholdinger (University Bonn). This project was carried out in the framework of the priority program 2089. “Rhizosphere spatiotemporal organization—a key to rhizosphere functions” funded by DFG, German Research Foundation (project number 470748155).

Financial support

Open Access funding enabled and organized by Projekt DEAL. This project was carried out in the framework of the priority program 2089. “Rhizosphere spatiotemporal organization—a key to rhizosphere functions” funded by DFG, German Research Foundation (project number 470748155).

References

Adamczewski, R. and Zarebanadkouki, M.: Tum-Soil-Biophysics/RWU_NeutronRadiographyD2O_InverseModelling: ImageProcessing-InverseModelling, , https://doi.org/10.5281/zenodo.19253776, 2026.

Adamczewski, R., Kaestner, A., and Zarebanadkouki, M.: Rhizosphere hydraulic regulation in maize: tailoring rhizosphere properties to varying soil textures and moistures, Plant Soil, 509, 53–66, https://doi.org/10.1007/s11104-024-06840-2, 2025.

Ahmed, M. A., Zarebanadkouki, M., Kaestner, A., and Carminati, A.: Measurements of water uptake of maize roots: the key function of lateral roots, Plant Soil, 398, 59–77, https://doi.org/10.1007/s11104-015-2639-6, 2016.

Ahmed, M. A., Zarebanadkouki, M., Meunier, F., Javaux, M., Kaestner, A., and Carminati, A.: Root type matters: measurement of water uptake by seminal, crown, and lateral roots in maize, Journal of Experimental Botany, 69, 1199–1206, https://doi.org/10.1093/jxb/erx439, 2018.

Bassiouni, M., Manzoni, S., and Vico, G.: Optimal plant water use strategies explain soil moisture variability, Advances in Water Resources, 173, 104405, https://doi.org/10.1016/j.advwatres.2023.104405, 2023.

Cai, G., Carminati, A., Abdalla, M., and Ahmed, M. A.: Soil textures rather than root hairs dominate water uptake and soil–plant hydraulics under drought, Plant Physiology, 187, 858–872, https://doi.org/10.1093/plphys/kiab271, 2021.

Carminati, A. and Javaux, M.: Soil Rather Than Xylem Vulnerability Controls Stomatal Response to Drought, Trends in Plant Science, 25, 868–880, https://doi.org/10.1016/j.tplants.2020.04.003, 2020.

Carminati, A., Zarebanadkouki, M., Kroener, E., Ahmed, M. A., and Holz, M.: Biophysical rhizosphere processes affecting root water uptake, Annals of Botany, 118, 561–571, https://doi.org/10.1093/aob/mcw113, 2016.

Doussan, C., Pierret, A., Garrigues, E., and Pagès, L.: Water uptake by plant roots: II - Modelling of water transfer in the soil root-system with explicit account of flow within the root system - Comparison with experiments, Plant and Soil, 283, 99–117, https://doi.org/10.1007/s11104-004-7904-z, 2006.

Draye, X., Kim, Y., Lobet, G., and Javaux, M.: Model-assisted integration of physiological and environmental constraints affecting the dynamic and spatial patterns of root water uptake from soils, Journal of Experimental Botany, 61, 2145–2155, https://doi.org/10.1093/jxb/erq077, 2010.

Frensch, J., Hsiao, T. C., and Steudle, E.: Water and solute transport along developing maize roots, Planta, 198, 348–355, https://doi.org/10.1007/BF00620050, 1996.

Guswa, A. J.: The influence of climate on root depth: A carbon cost-benefit analysis, Water Resour. Res., 44, https://doi.org/10.1029/2007WR006384, 2008.

Hayat, F., Zarebanadkouki, M., Ahmed, M. A., Buecherl, T., and Carminati, A.: Quantification of hydraulic redistribution in maize roots using neutron radiography, Vadose Zone Journal, 19, e20084, https://doi.org/10.1002/vzj2.20084, 2020.

Hazman, M. Y. and Kabil, F. F.: Maize root responses to drought stress depend on root class and axial position, J Plant Res, 135, 105–120, https://doi.org/10.1007/s10265-021-01348-7, 2022.

Hochholdinger, F., Park, W. J., Sauer, M., and Woll, K.: From weeds to crops: genetic analysis of root development in cereals, Trends in Plant Science, 9, 42–48, https://doi.org/10.1016/j.tplants.2003.11.003, 2004.

Hohenbrink, T. L., Jackisch, C., Durner, W., Germer, K., Iden, S. C., Kreiselmeier, J., Leuther, F., Metzger, J. C., Naseri, M., and Peters, A.: Soil water retention and hydraulic conductivity measured in a wide saturation range, Earth System Science Data, 15, 4417–4432, https://doi.org/10.5194/essd-15-4417-2023, 2023.

Klein, S. P., Schneider, H. M., Perkins, A. C., Brown, K. M., and Lynch, J. P.: Multiple Integrated Root Phenotypes Are Associated with Improved Drought Tolerance1 [OPEN], Plant Physiology, 183, 1011–1025, https://doi.org/10.1104/pp.20.00211, 2020.

Landsberg, J. J. and Fowkes, N. D.: Water Movement Through Plant Roots, Ann Bot, 42, 493–508, https://doi.org/10.1093/oxfordjournals.aob.a085488, 1978.

Lippold, E., Phalempin, M., Schlüter, S., and Vetterlein, D.: Does the lack of root hairs alter root system architecture of Zea mays?, Plant Soil, 467, 267–286, https://doi.org/10.1007/s11104-021-05084-8, 2021.

Lynch, J. P.: Steep, cheap and deep: an ideotype to optimize water and N acquisition by maize root systems, Annals of Botany, 112, 347–357, https://doi.org/10.1093/aob/mcs293, 2013.

Lynch, J. P., Galindo-Castañeda, T., Schneider, H. M., Sidhu, J. S., Rangarajan, H., and York, L. M.: Root phenotypes for improved nitrogen capture, Plant Soil, 502, 31–85, https://doi.org/10.1007/s11104-023-06301-2, 2024.

Meunier, F., Zarebanadkouki, M., Ahmed, M. A., Carminati, A., Couvreur, V., and Javaux, M.: Hydraulic conductivity of soil-grown lupine and maize unbranched roots and maize root-shoot junctions, J. Plant Physiol., 227, 31–44, https://doi.org/10.1016/j.jplph.2017.12.019, 2018.

Moradi, A. B., Carminati, A., Vetterlein, D., Vontobel, P., Lehmann, E., Weller, U., Hopmans, J. W., Vogel, H.-J., and Oswald, S. E.: Three-dimensional visualization and quantification of water content in the rhizosphere, New Phytologist, 192, 653–663, https://doi.org/10.1111/j.1469-8137.2011.03826.x, 2011.

Passioura, J. B.: Water Transport in and to Roots, Annual Review of Plant Biology, 39, 245–265, https://doi.org/10.1146/annurev.pp.39.060188.001333, 1988.

Perktold, J., Seabold, S., Sheppard, K., ChadFulton, Shedden, K., jbrockmendel, j-grana6, Quackenbush, P., Arel-Bundock, V., McKinney, W., Langmore, I., Baker, B., Gommers, R., yogabonito, s-scherrer, Zhurko, Y., Brett, M., Giampieri, E., yl565, Millman, J., Hobson, P., Vincent, Roy, P., Augspurger, T., tvanzyl, alexbrc, Hartley, T., Perez, F., Tamiya, Y., and Halchenko, Y.: statsmodels/statsmodels: Release 0.14.2, , https://doi.org/10.5281/zenodo.10984387, 2024.

Poorter, L., McDonald, I., Alarcón, A., Fichtler, E., Licona, J.-C., Peña-Claros, M., Sterck, F., Villegas, Z., and Sass-Klaassen, U.: The importance of wood traits and hydraulic conductance for the performance and life history strategies of 42 rainforest tree species, New Phytologist, 185, 481–492, https://doi.org/10.1111/j.1469-8137.2009.03092.x, 2010.

Steudle, E.: Water transport across roots, Plant Soil, 167, 79–90, https://doi.org/10.1007/BF01587602, 1994.

Steudle, E.: Water uptake by roots: effects of water deficit, Journal of Experimental Botany, 51, 1531–1542, https://doi.org/10.1093/jexbot/51.350.1531, 2000.

Steudle, E. and Frensch, J.: Osmotic responses of maize roots, Planta, 177, 281–295, https://doi.org/10.1007/BF00403585, 1989.

Tötzke, C., Kardjilov, N., Hilger, A., Rudolph-Mohr, N., Manke, I., and Oswald, S. E.: Three-dimensional in vivo analysis of water uptake and translocation in maize roots by fast neutron tomography, Sci Rep, 11, 10578, https://doi.org/10.1038/s41598-021-90062-4, 2021.

Vetterlein, D., Lippold, E., Schreiter, S., Phalempin, M., Fahrenkampf, T., Hochholdinger, F., Marcon, C., Tarkka, M., Oburger, E., Ahmed, M., Javaux, M., and Schlüter, S.: Experimental platforms for the investigation of spatiotemporal patterns in the rhizosphere—Laboratory and field scale, Journal of Plant Nutrition and Soil Science, 184, 35–50, https://doi.org/10.1002/jpln.202000079, 2021.

Vetterlein, D., Phalempin, M., Lippold, E., Schlüter, S., Schreiter, S., Ahmed, M. A., Carminati, A., Duddek, P., Jorda, H., Bienert, G. P., Bienert, M. D., Tarkka, M., Ganther, M., Oburger, E., Santangeli, M., Javaux, M., and Vanderborght, J.: Root hairs matter at field scale for maize shoot growth and nutrient uptake, but root trait plasticity is primarily triggered by texture and drought, Plant Soil, 478, 119–141, https://doi.org/10.1007/s11104-022-05434-0, 2022.

Virtanen, P., Gommers, R., Oliphant, T. E., Haberland, M., Reddy, T., Cournapeau, D., Burovski, E., Peterson, P., Weckesser, W., Bright, J., van der Walt, S. J., Brett, M., Wilson, J., Millman, K. J., Mayorov, N., Nelson, A. R. J., Jones, E., Kern, R., Larson, E., Carey, C. J., Polat, İ., Feng, Y., Moore, E. W., VanderPlas, J., Laxalde, D., Perktold, J., Cimrman, R., Henriksen, I., Quintero, E. A., Harris, C. R., Archibald, A. M., Ribeiro, A. H., Pedregosa, F., and van Mulbregt, P.: SciPy 1.0: fundamental algorithms for scientific computing in Python, Nat Methods, 17, 261–272, https://doi.org/10.1038/s41592-019-0686-2, 2020.

Wankmüller, F. J. P., Delval, L., Lehmann, P., Baur, M. J., Cecere, A., Wolf, S., Or, D., Javaux, M., and Carminati, A.: Global influence of soil texture on ecosystem water limitation, Nature, 635, 631–638, https://doi.org/10.1038/s41586-024-08089-2, 2024.

Warren, J. M., Bilheux, H., Kang, M., Voisin, S., Cheng, C.-L., Horita, J., and Perfect, E.: Neutron imaging reveals internal plant water dynamics, Plant Soil, 366, 683–693, https://doi.org/10.1007/s11104-012-1579-7, 2013.

Zarebanadkouki, M., Kim, Y. x., Moradi, A. b., Vogel, H.-J., Kaestner, A., and Carminati, A.: Quantification and Modeling of Local Root Water Uptake Using Neutron Radiography and Deuterated Water, Vadose Zone Journal, 11, vzj2011.0196, https://doi.org/10.2136/vzj2011.0196, 2012.

Zarebanadkouki, M., Kim, Y. X., and Carminati, A.: Where do roots take up water? Neutron radiography of water flow into the roots of transpiring plants growing in soil, New Phytologist, 199, 1034–1044, https://doi.org/https://doi.org/10.1111/nph.12330, 2013a.

Zarebanadkouki, M., Kim, Y. X., and Carminati, A.: Where do roots take up water? Neutron radiography of water flow into the roots of transpiring plants growing in soil, New Phytologist, 199, 1034–1044, https://doi.org/10.1111/nph.12330, 2013b.

Zarebanadkouki, M., Kroener, E., Kaestner, A., and Carminati, A.: Visualization of Root Water Uptake: Quantification of Deuterated Water Transport in Roots Using Neutron Radiography and Numerical Modeling, Plant Physiology, 166, 487–499, https://doi.org/10.1104/pp.114.243212, 2014.

Zarebanadkouki, M., Meunier, F., Couvreur, V., Cesar, J., Javaux, M., and Carminati, A.: Estimation of the hydraulic conductivities of lupine roots by inverse modelling of high-resolution measurements of root water uptake, Ann Bot, 118, 853–864, https://doi.org/10.1093/aob/mcw154, 2016a.

Zarebanadkouki, M., Ahmed, M. A., and Carminati, A.: Hydraulic conductivity of the root-soil interface of lupin in sandy soil after drying and rewetting, Plant Soil, 398, 267–280, https://doi.org/10.1007/s11104-015-2668-1, 2016b.

Zarebanadkouki, M., Trtik, P., Hayat, F., Carminati, A., and Kaestner, A.: Root water uptake and its pathways across the root: quantification at the cellular scale, Sci Rep, 9, 12979, https://doi.org/10.1038/s41598-019-49528-9, 2019.

Zhan, A., Schneider, H., and Lynch, J. P.: Reduced Lateral Root Branching Density Improves Drought Tolerance in Maize, Plant Physiology, 168, 1603–1615, https://doi.org/10.1104/pp.15.00187, 2015.

Zwieniecki, M. A., Thompson, M. V., and Holbrook, N. M.: Understanding the Hydraulics of Porous Pipes: Tradeoffs Between Water Uptake and Root Length Utilization, J Plant Growth Regul, 21, 315–323, https://doi.org/10.1007/s00344-003-0008-9, 2002a.

Zwieniecki, M. A., Thompson, M. V., and Holbrook, N. M.: Understanding the hydraulics of porous pipes: Tradeoffs between water uptake and root length utilization, Journal of Plant Growth Regulation, 21, 315–323, https://doi.org/10.1007/s00344-003-0008-9, 2002b.